Solar chromospheric heating by magnetohydrodynamic waves: dependence on magnetic field inclination

Mayu Koyama[1,2] and Toshifumi Shimizu[2,1]

[1]*Department of Earth and Planetary Science, The University of Tokyo,*

7-3-1 Hongo, Bunkyo-ku, Tokyo 113-0033, Japan

[2]*Institute of Space and Astronautical Science, Japan Aerospace Exploration Agency,*

3-1-1 Chuo-ku, Sagamihara, Kanagawa 252-5210, Japan

ABSTRACT

A proposed mechanism for solar chromospheric heating is that magnetohydrodynamic waves propagate upward along magnetic field lines and dissipate their energy in the chromosphere. In particular, compressible magneto-acoustic waves may contribute to the heating. Theoretically, the components below the cutoff frequency cannot propagate into the chromosphere; however, the cutoff frequency depends on the inclination of the magnetic field lines. In this study, using high temporal cadence spectral data of IRIS and Hinode SOT spectropolarimeter (SP) in plages, we investigated the dependence of the low-frequency waves on magnetic-field properties and quantitatively estimated the amount of energy dissipation in the chromosphere. The following results were obtained: (a) The amount of energy dissipated by the low-frequency component (3–6 mHz) increases with the field inclination below 40 degrees, whereas it is decreased as a function of the field inclination above 40 degrees. (b) The amount of the energy is enhanced toward 10^4 W/m^2, which is the energy required for heating in the chromospheric plage regions, when the magnetic field is higher than 600 G and inclined more than 40 degree. (c) In the photosphere, the low-frequency component has much more power in the magnetic field inclined more and weaker than 400 G. The results suggest

that the observed low-frequency components can bring the energy along the magnetic field lines and that only a specific range of the field inclination angles and field strength may allow the low-frequency component to bring the sufficient amount of the energy into the chromosphere.

1. INTRODUCTION

The solar chromosphere is the dynamical and thin atmosphere formed above the solar surface (photosphere); it has a temperature of approximately 10,000 K, higher than that of the photosphere (6,000 K). The amount of energy required to retain the chromospheric temperature is 10^4 W/m^2 for active regions, an order of magnitude larger than the heating for the solar corona, which is the lower-density atmosphere heated to over 1 MK beyond the magnetic structures of chromosphere (Withbroe & Noyes 1977). The physical mechanisms responsible for transferring the energy to the chromosphere and the corona and dissipating it there are still in debate. The major candidates are magnetohydrodynamic (MHD) waves and nanoflares. The turbulent convective gas motions at the photosphere excite MHD waves propagating to the chromosphere and the corona along the magnetic field lines (e.g., a review by Jess 2023, and references therein), whereas they generate tangential discontinuity and braiding in magnetic field lines in the corona, leading to numerous tiny magnetic reconnection events (e.g., a review by Pontin & Hornig 2020, and references therein), so-called nanoflares (Parker 1988). Both mechanisms are closely associated with dynamical behaviors of the magnetic field lines in the solar atmosphere.

Compressible magneto-acoustic waves may be evolved to shock waves due to steepening, and their dissipation may contribute to the heating of the atmosphere. Therefore, investigating the propagation of magneto-acoustic waves in the low atmosphere to understand their roles in chromospheric heating is important. There are two types of magneto-acoustic waves: fast mode—in which the phase relation between the gas pressure and magnetic pressure is in-phase—and slow mode—in which the phase

relation between the gas pressure and magnetic pressure are in the opposite phase. The slow mode propagates along magnetic field lines. In the presence of a magnetic field, sunspots are the most apparent regions for typical display of oscillations in intensity and Doppler velocity. The power spectra are dominated for 5 min (approximately 3 mHz) in the photosphere and 3 min (approximately 5 mHz or higher) in the chromosphere (Centeno et al. 2009). The oscillations in the umbrae and penumbrae of sunspots have been generally interpreted as MHD waves. Kanoh et al. (2016) conducted simultaneous observations of the Hinode and IRIS satellites and showed the existence of the slow mode waves in a sunspot umbra based on the phase relation of waves observed at the photosphere and the chromosphere. In addition, the energy flux in each layer was derived and the energy dissipation was estimated from the difference. They obtained an energy flux of 8.3×10 W/m^2 for waves in the upper chromosphere and 2.0×10^4 W/m^2 for the photosphere, demonstrating that the difference is sufficient to heat the chromosphere. Oscillating signatures in sunspot penumbrae, known as running penumbral waves, are interpreted as upward propagating slow-model waves guided by the magnetic field lines (Löhner-Böttcher & Bello González 2015). The dominant frequency of the waves changes toward lower values as one moves from the umbral center to the surroundings where the magnetic fields are more inclined to the surface (Bloomfield et al. 2007; Jess et al. 2013).

The critical frequency at which a wave can propagate is called the cutoff frequency; it is defined as $\nu_{ac} = \frac{\gamma g}{4\pi c_s}$, where c_s is the sound speed, γ is the specific heat ratio of a monatomic molecule, and g is the gravitational acceleration (Priest 2014). The cutoff frequency is at its maximum in the lowest temperature layer, i.e., the temperature minimum, clearly shown as the height variation of the cutoff frequency in observations of a sunspot umbra (Felipe et al. 2018) and in numerical models (Felipe & Sangeetha 2020). The low-frequency waves below the frequency cannot propagate into the chromosphere. In the quiet Sun, where the plasma β is much larger than 1, the cutoff frequency is approximately 5.2 mHz ($\gamma = 5/3$, $g = 274$m/s, $c_s = 7$ km/s). Bel & Leroy (1977) showed theoretically that the cutoff frequency depends on the structure of the magnetic field. In the region of strong magnetic field ($\beta < 1$), the cutoff frequency depends on the inclination angle of the magnetic field lines with respect to the solar surface. This is because the effective gravity on the

magnetic field lines changes, and the cutoff frequency becomes

$$\nu_{ac} = \frac{\gamma g \cos\theta}{4\pi c_s}. \tag{1}$$

Note that the cutoff frequency given in equation (1) is only applicable in an isothermal atmosphere and different forms of the cut-off frequency are inferred from various representations of the wave equation depending on choice of variables in more general atmospheres (Schmitz & Fleck 1998). McIntosh & Jefferies (2006) observed that low-frequency magneto-acoustic waves below the cutoff frequency (5.2 mHz) propagate into the chromosphere in the sunspot penumbra where the magnetic field is highly tilted to the surface. Numerical simulations of wave propagation in the low atmosphere also show that the magnetic field inclination is crucial for the propagation of low-frequency waves through dynamic magnetic structures (Heggland et al. 2011) and wave energy flux (Schunker & Cally 2006; Cally & Moradi 2013).

For observationally investigating the significance of wave contributions to the upper atmosphere, quantitatively estimating the amount of energy magneto-acoustic waves transported from the photosphere to the chromosphere and deposited in the chromosphere considering the magnetic field environment is essential. However, the number of studies on magnetic plages outside sunspots is largely limited. Sobotka et al. (2016) used the Interferometric Bidimensional Spectrometer (IBIS; Cavallini 2006) at the Dunn Solar Telescope (DST) to evaluate the deposited acoustic energy flux from the power spectra of Doppler oscillations measured in the Ca II 853.2 nm line core in comparison to the radiative loss. In active areas around sunspots, the amount of energy dissipated by 4–9 mHz waves was estimated to be up to 5×10^3 W/m^2 in the height range 1000–1500 km from the solar surface (the middle chromosphere). The estimated flux is slightly insufficient to heat the chromosphere; however, the heating contribution was revealed to increase from 23 % in chromosphere network to 54 % in a plage. Abbasvand et al. (2020a) used observations of the Ca II 854.2 nm, Hα and Hβ lines with the Fast Imaging Solar Spectrograph (FISS; Chae et al. 2013) at the 1.6-m Goode Solar Telescope and the echelle spectrograph attached to the German Vacuum Tower Telescope (von der Lühe 1998) and derived that the acoustic energy flux at frequencies up to 20 mHz deposited in the heights from

1000 to 1400 km can be balanced by the radiative loss in a quiet region, but the deposited acoustic flux is insufficient in the upper chromosphere higher than 1400 km in both quiet and plage regions. Abbasvand et al. (2020b) used observations of the Ca II 854.2-nm line with the IBIS and derived the acoustic energy flux in the plage, demonstrating that it contributes by $50\% - 60\%$ in locations with vertical magnetic field and $70\% - 90\%$ in regions where the magnetic field is inclined more than $50°$ to the solar surface normal.

In this study, we investigate roles of magnetic field properties in oscillations observed in plages, which are observed brightly in the chromosphere; consequently, heating is inferred to be relatively high so that we could understand more details of energy transport and dissipation by waves. For quantitative understanding, we estimate the energy dissipation in the chromosphere by comparing the energy flux at three altitudes in the plages: the photosphere, lower chromosphere, and upper chromosphere. In addition, as the cutoff frequency varies depending on the magnetic-field structure of the photosphere, we estimate the energy dissipation in the chromosphere including the energy flux due to low-frequency waves (less than 5 mHz) below the cutoff frequency. Determining the inclination of the magnetic field lines with respect to the solar surface with the Hinode SOT/SP, we verify whether low-frequency waves below the cutoff frequency propagate into the chromosphere depending on the inclination of the magnetic field lines. We describe observational methodologies in Section 2. Section 3 shows the observational results, and Section 4 discusses the interpretation of the observation results. A summary of this paper is given in Section 5.

2. OBSERVATIONS AND DATA ANALYSIS

Simultaneous observations of the plage region were performed by the Solar Optical Telescope (SOT) (Tsuneta et al. 2008; Suematsu et al. 2008; Shimizu et al. 2008; Ichimoto et al. 2008) onboard the Hinode satellite (Kosugi et al. 2007) and the IRIS satellite (De Pontieu et al. 2014) for approximately one hour each day on February 9–12, 2018. The observations were carried out along with the observation proposal named IRIS-Hinode Operation Plan (IHOP) 0341. The period of each simultaneous Hinode and IRIS observation and the heliocentric coordinate of the center of the leftmost IRIS slit are shown in Table 1. Each observation region covers a plage region between the leading

and following sunspots in active region NOAA 12699. The observation area on February 10, 2018, as an example, is shown in Figure 1. The blue frame shows the SOT field of view, whereas the red lines show the slit positions of IRIS.

Table 1. Coordinated observation period and coordinate

Date	Time (UT)	Position (x, y)
09 February 2018	$12{:}59{:}10 - 14{:}09{:}58$	$(-335'', -17'')$
10 February 2018	$11{:}35{:}13 - 12{:}44{:}33$	$(-122'', -9'')$
11 February 2018	$12{:}05{:}11 - 13{:}09{:}32$	$(104'', -4'')$
12 February 2018	$01{:}05{:}11 - 02{:}14{:}32$	$(226'', -5'')$
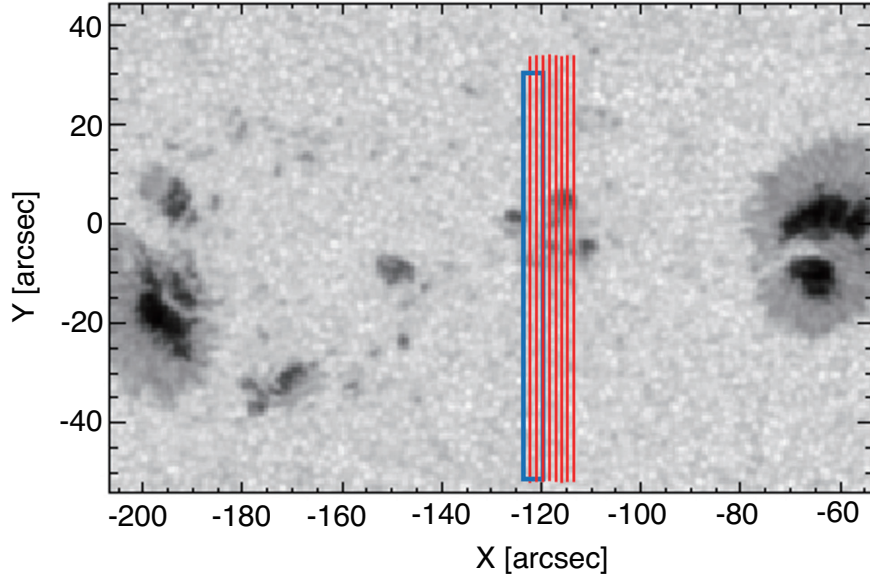
Figure 1. Observation area on 10 February 2018. Blue frame shows the field of view captured by the Hinode SOT observation, whereas red lines show the slit positions for the IRIS observation. The IRIS slit positions are 8 steps at $1''$ intervals. The SOT field of view contains 10 slit positions of the spectro-polarimeter measurement with 0.3" interval.

2.1. *Hinode SOT observation and analysis*

The SOT observations were carried out by a spectro-polarimeter (SP) (Lites et al. 2013) that recorded four Stokes (I, Q, U, V) profiles of Fe I lines at 6301.5Å and 6302.5Å with a spectral sampling

of 21.55 mÅ. The field of view is $3'' \times 82''$ with 10 slit positions for a $3''$ width at $0.3''$ interval. The Stokes parameters were measured with exposures during the continuous rotation of the polarization modulator in 1.6 s at each slit position, and it takes approximately 21 s to scan the file of view. This is the fast-mapping mode, wherein the exposures were accumulated at two slit positions with a slit width of $0.15''$; the two pixels were summed in the slit direction to provide spectral data with a pixel size of $0.32''$. In this analysis, we used the level-2 data from the Community Spectro-polarimetric Analysis Center (CSAC) at HAO/NCAR [1]. The data was calibrated with the SP_PREP routine in Solar SoftWare (SSW) (Lites & Ichimoto 2013), followed by an inversion assuming a Milne–Eddington atmosphere with the HAO MERLIN code to obtain physical quantities such as magnetic field strength, azimuth angle, and tilt relative to the line-of-sight direction.

For the magnetic field strength, the line-of-sight component was used in the analysis, and the inclination was analyzed using the inclination of the magnetic field lines from the local zenith of the photosphere. The field inclination was transformed from the line-of-sight coordinate system to the local coordinate system. We adopted the angle at which the field inclination becomes small relative to the local zenith due to the 180° ambiguity resolution because the magnetic field lines are expected to continuously tilt from the center of the pore to the periphery.

2.2. *IRIS observation and analysis*

IRIS was observed with the slit (width $0.166''$) for spectroscopy and with the slit jaw imager (SJI), which measures the radiation intensity by imaging observations. The time variation of the Doppler velocity was derived from spectroscopic observations of the Mg II k line. The spectral sampling is 12.72mÅ, and the time resolution is 27 s. The slit scanned a $7''$ width in 8 steps at $1''$ intervals. The SJI was acquired every 14 s at four wavelengths: C II 1330Å, Si IV 1400Å, Mg II k 2796Å, and Mg II wing 2830Å. The SJI enabled the identification of the exact position of the slit. We used the level-2 data created with the instrumental calibration including the dark current subtraction, flat field, and geometrical corrections (De Pontieu et al. 2014).

[1] https://www2.hao.ucar.edu/csac

The wing of the Mg II k line provides information about the lower part of the chromosphere, whereas the core is sensitive to the upper part of the chromosphere (Leenaarts et al. 2013a,b, Pereira et al. 2013). The Mg II k line is typically observed in double peaks in the quiet-Sun and single peaks in sunspots. The plage may show different shapes, with brighter, wider wings, single peaks, or inverted cores (Morrill et al. 2001). The depth of the core inversion is inversely proportional to the magnetic field strength. This is because the Mg II k line is a very abundant elemental resonance line; therefore, the line core is optically thick and can form at relatively low densities in nonlocal thermodynamic equilibrium (Carlsson et al. 2015, Schmit et al. 2015).

The bisector method was used to derive the wavelength of the line center at the intensity level of the line wings; it is the midpoint of λ_1 and λ_2 defined at 40% of the peak intensity of Mg II k, as shown in Figure 2(a) (Graham & Cauzzi 2015). The reference wavelength for the zero Doppler velocity is derived by averaging the line profiles averaged in the spatial and temporal directions for all pixels on each day. The quiet Sun is expected to have intrinsic velocity of zero or less than a few km/s. However, as we did not obtain data for the quiet Sun in this observation, we assume that the velocity is zero, averaged over the observation region in the spatial and temporal directions. The Doppler velocity was obtained from the deviation of the wavelength from the reference wavelength.

The wavelength of the line core was defined by detecting three extremes k_1, k_2, k_3 (k_3 is the minimum value between k_1 and k_2) and applying Gaussian fitting in the range from k_1 to k_2 (Figure 2(b)). In the plage region, Mg II k may be observed as a single peak with a tiny core inverted profile, as shown in Figure 2(c). In such cases, profiles where (intensity decrease at k_3)/(average of the intensities with respect to k_1 and k_2) is less than 15% are considered to be at single peaks, and the wavelength was derived with the Gaussian fit to the whole line profile instead.

2.3. Co-alignment of spectral lines

The Hinode SOT/SP and IRIS fields of view were aligned to identify the IRIS slit positions on the SP field of view. The SJI images of Mg II wing (2832Å), which are dominantly photospheric, were used for the alignment. Each image was cross-correlated with the SP map taken at the closest time, providing the relative displacement between them.
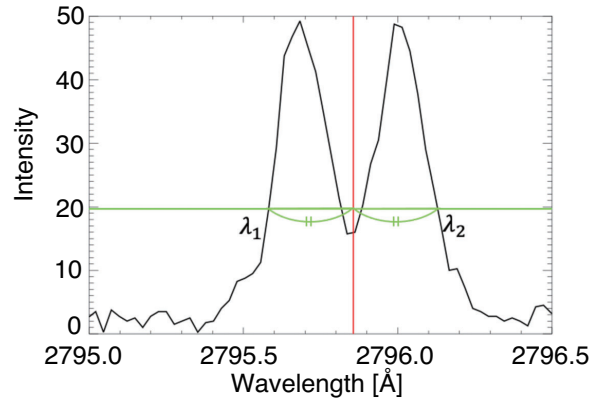
(a) wing
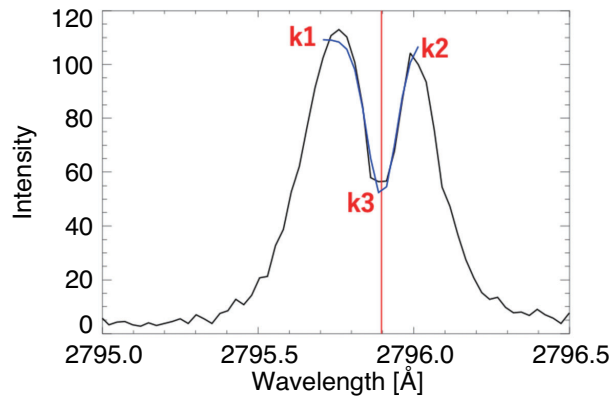
(b) core
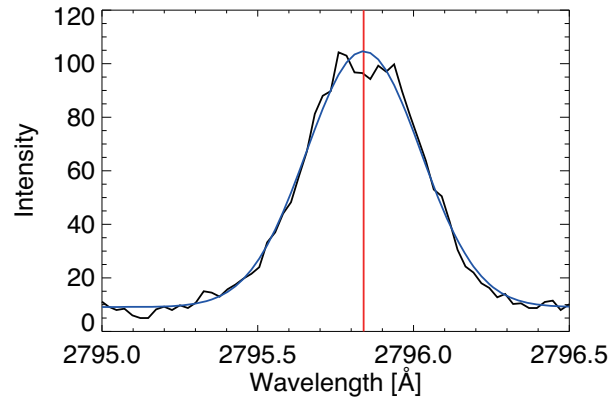
(c) core (single peak)

Figure 2. Analysis for Mg II k to derive line-of-sight velocity. (a) The bisector at 40% of the peak intensity for velocity at the lower chromosphere. (b) The Gaussian fitting to a core inverted profile for velocity at the upper chromosphere. (c) The Gaussian fitting to the whole line profile is used instead if the core inverted profile is tiny.

Figure 3 shows how the SP and IRIS fields of view were drifted in the X, i.e., E-W direction on the solar surface as a function of the time. At least two IRIS slits are included in SP field of view. IRIS slits in the SP field-of-view were selected, and SP pixel data overlapping with the selected slits were used for analysis. The positions in the N-S direction were also co-aligned in the same manner.
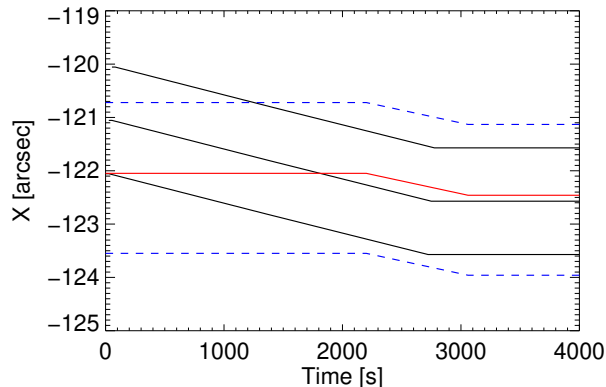

Figure 3. SP and IRIS fields of view in the x-direction as a function of time. Black line: the slit position of the three IRIS slits located within the SP field of view. Blue dotted lines: the ends of SP field of view. Red line: the center of SP field of view. The figure is for the data captured on February 10, 2018.

3. RESULTS

The line-of-sight magnetic field strength and the inclination of the magnetic field in the observation regions are shown in Figures 4 and 5. The inclination of the magnetic field, denoted by θ, is defined in the local frame coordinate, i.e., $0°$ in the normal direction of the solar surface and $90°$ in the horizontal direction. From the negative polarity of $y = 20'' - 25''$ in Figure 5, the magnetic field lines are continuously inclined from the center of the pore (a small sunspot with no penumbra), where the magnetic field strength is relatively strong, to the surroundings. Pixels with the degree of polarization of less than 1%, which are considered unsuitable for Stokes profile inversion with good accuracy, were not used in the analysis.

Figure 6 shows an example of the time series of the Doppler velocities observed in a pixel on February 10, 2018. The pixel has a weak magnetic field strength (353 G) and tilted magnetic field lines ($\theta = 54°$). The amplitudes in each layer are observed to be within 0.8 km/s in the photosphere,

approximately 2 km/s in the lower chromosphere, and up to 10 km/s in the upper chromosphere. The amplitude of the waves is larger in the upper layers. This is because the density decreases in the upper layers. We derived the power distribution by Fourier transforming each wave because determining the phase difference from the waves observed in each layer is difficult.
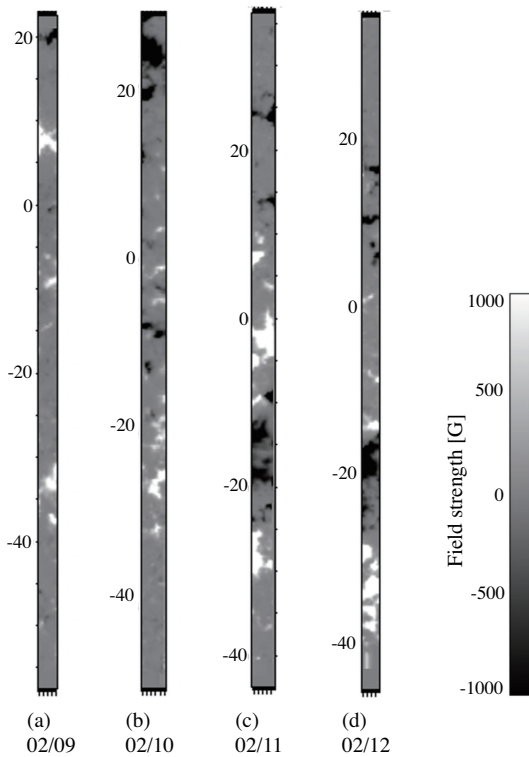

Figure 4. LOS magnetic field strength. The unit on the vertical axis is arcsec.

3.1. *Dependence of power spectrum on inclination of magnetic field lines*

The Fourier transform was applied to the time profiles to derive the power distribution as a function of the frequency. Figure 7 shows the power spectrum for the three sets of time profiles: (a) in the photosphere derived from the SP data, (b) in the lower chromosphere derived from the wing of the Mg II k line in IRIS, and (c) in the upper chromosphere derived from the core. The power spectra are the averages of the five-day data. The inclination of the magnetic field lines θ is classified into $0° < \theta < 30°$, $30° < \theta < 50°$, and $50° < \theta < 90°$. For all data, a subsonic filter (Title et al. 1989, Oba et al. 2017) was applied before the Fourier transfer to remove the frequency component caused by
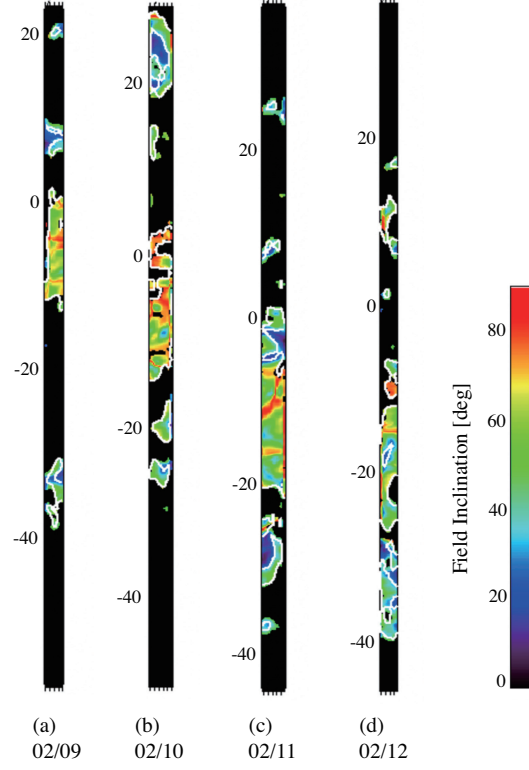
Figure 5. Inclination of magnetic field lines. The unit on the vertical axis is arcsec.

the gas convection at the photosphere. The power distribution below 1.5 mHz was removed because the gas convection is below 2 mHz. Figure 7(a) shows that the power distribution in photosphere is enhanced at 3 mHz. This may be due to the observation of the 5-min oscillations (3.3 mHz). Below 5 mHz, there is no difference in the power with respect to the inclination of the magnetic field lines, while above 5 mHz, the power of $\theta > 30°$ is slightly larger than that of $\theta < 30°$. As shown in Figure 7(b), in the lower chromosphere, the power of $\theta > 50°$ is smaller than the others below 5 mHz, and there is no difference with respect to the inclination of the magnetic field lines above 5 mHz. Figure 7(c) shows that the power of $\theta > 50°$ in the upper part of the chromosphere is smaller than the others for all frequencies.
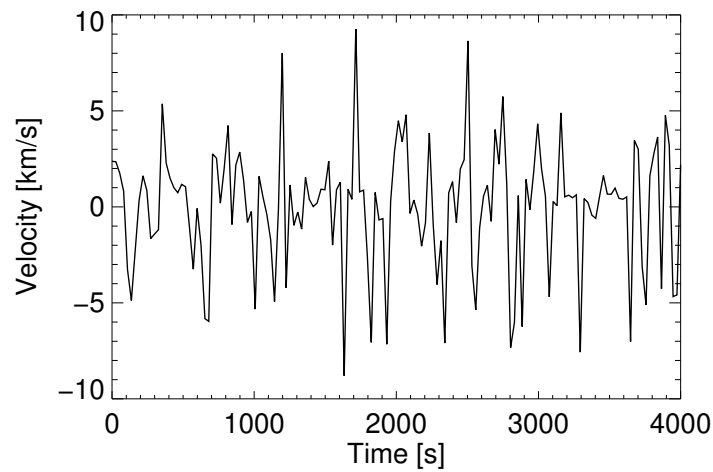
3.2. *Energy dissipation in the photosphere and chromosphere*
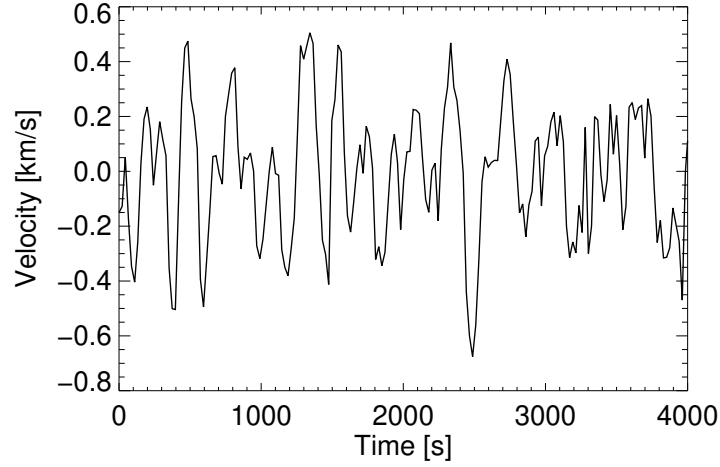
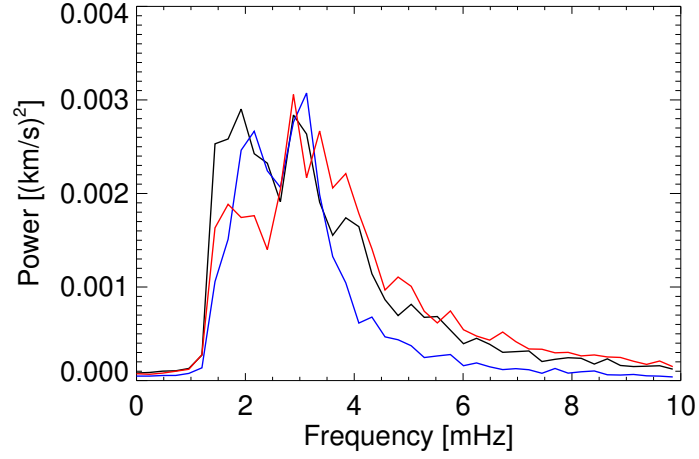(a) In the photosphere derived from the SP data
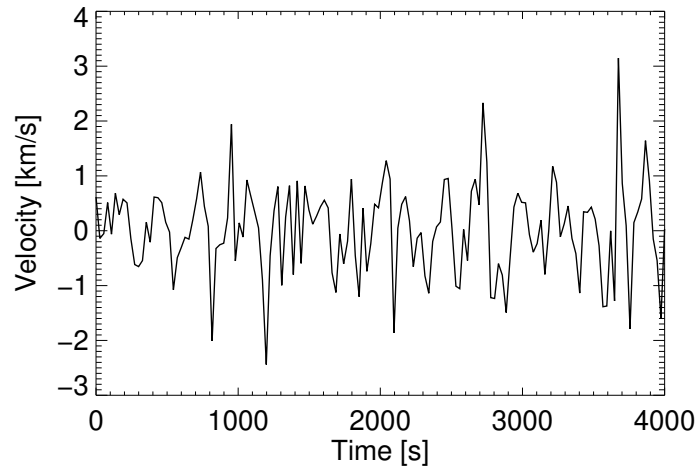
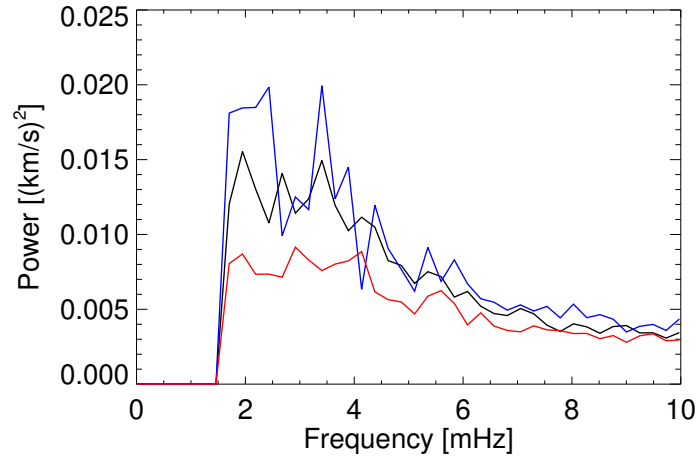(b) In the lower chromosphere derived from IRIS Mg II k wing

(c) In the upper chromosphere derived from IRIS Mg II k core
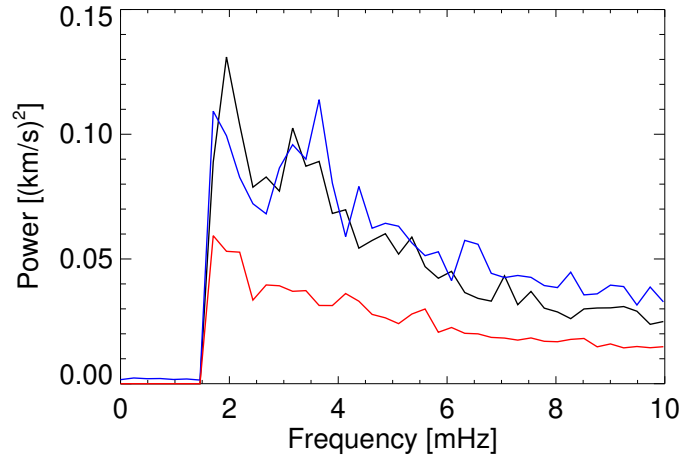
Figure 6. Time series of the Doppler velocity observed in a pixel region on February 10, 2018.

(a) In the photosphere derived from the SP data

(b) In the lower chromosphere derived from IRIS Mg Ⅱ k wing

(c) In the upper chromosphere derived from IRIS Mg Ⅱ k core

Figure 7. Power distribution as a function of the frequency. The inclination of the magnetic field lines; blue lines show $0° < \theta < 30°$, black lines show $30° < \theta < 50°$, red lines show $50° < \theta < 90°$.

The energy flux F for the three heights at the photosphere, lower and upper chromosphere, can be estimated using the following equation (cf. Sobotka et al. 2016)

$$F = \int_{\nu_{ac}}^{\nu_{max}} \rho P_v(\nu) v_g(\nu) d\nu \tag{2}$$

where ρ is the density, $P_v(\nu)$ is the power spectrum of the Doppler velocity obtained from the Fourier transform, and v_g is the group velocity for propagating waves. The group velocity for waves propagating along inclined magnetic field lines is given by the following equation using the cutoff frequency ν_{ac} obtained from Equation (1) and the sound speed $c_s = \sqrt{\gamma p/\rho}$,

$$v_g = c_s \sqrt{1 - (\nu_{ac}/\nu)^2}. \tag{3}$$

Here the acoustic slow wave is essentially field-guided (Schunker & Cally 2006) and we therefore multiply the geometric factor $\cos\theta$ in the calculation of the energy flux, in order to derive the energy flux which the acoustic waves bring in the vertical direction upward from the solar surface. The density ρ and temperature T at each height are taken from the atmospheric model VAL-F (Vernazza et al. 1981), which is an atmospheric model for bright inter-network regions.

The energy dissipation at the photosphere was estimated from the difference between the lower chromosphere and the photosphere, while the energy dissipation at the chromosphere was estimated from the difference between the upper and lower chromospheres. The error is obtained from the following equation using the power spectrum error σ_{P_v}.

$$\sigma_F = \sqrt{\sum_v (\rho v_g)^2 (\sigma_{P_v})^2} \tag{4}$$

3.2.1. Dependence on the inclination of magnetic field

The average amounts of energy dissipated in the photosphere and chromosphere are shown in Figure 8(b) and Figure 8(a), respectively, as a function of the inclination of the magnetic field. The inclination is measured at the photosphere (Figure 5). The red line represents the amount of energy dissipated by low frequency (3–6 mHz) component, while the black line represents the amount of energy dissipated by high frequency (6–10 mHz) component. The inclination of the magnetic field lines θ is classified into $\theta < 30°$, 5° each for $30° < \theta < 60°$, and $\theta > 60°$.

(a)

In the chromosphere
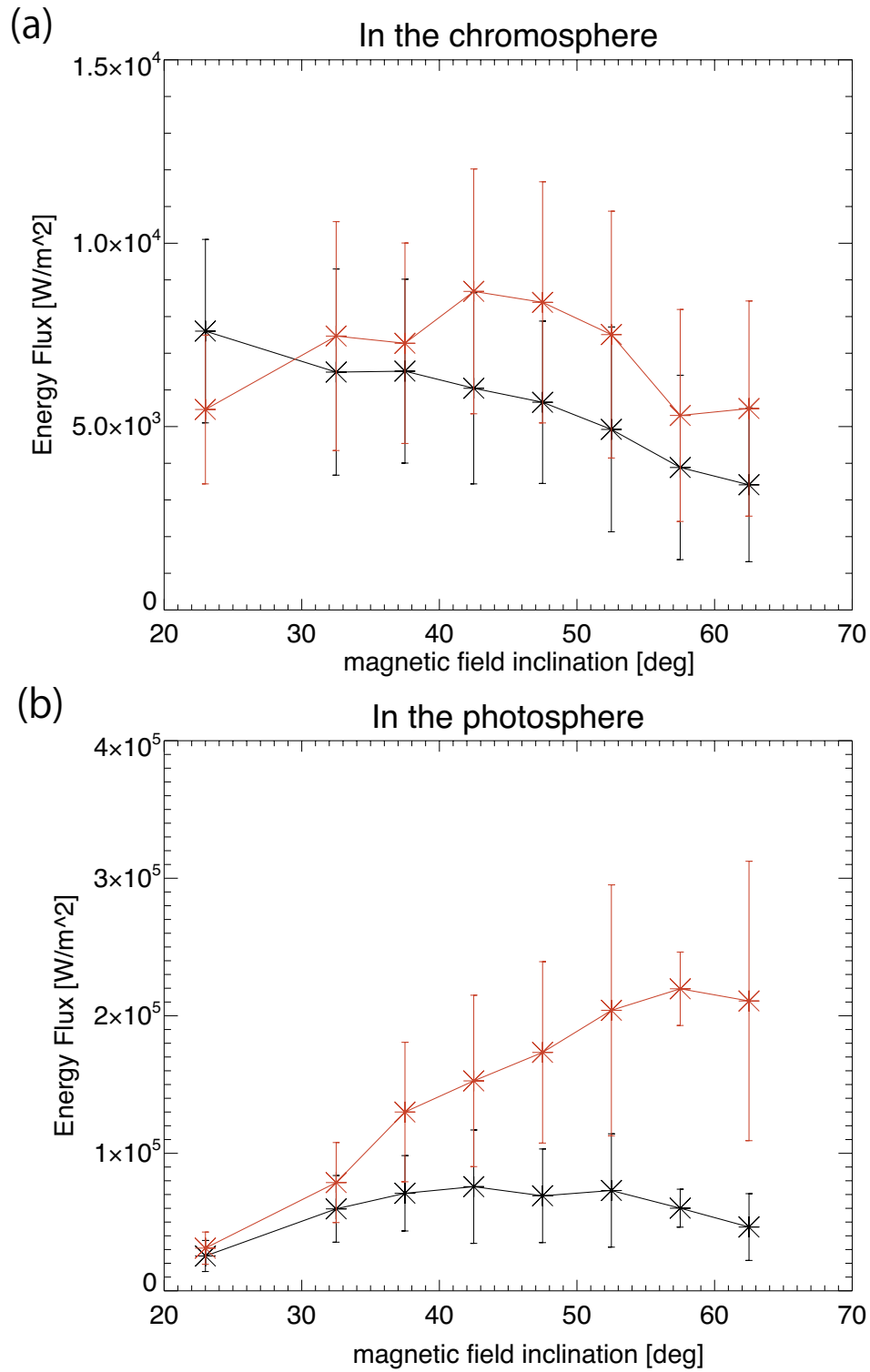

(b)

In the photosphere

Figure 8. The average amount of energy dissipated (a) in the chromosphere and (b) in the photosphere as a function of the inclination of the magnetic field lines. Red line: low frequency (3–6 mHz), Black line: high frequency (6–10 mHz).

In the photosphere, the low-frequency waves make more contributions to the energy dissipation. The energy by low-frequency waves increases monotonically with the field inclination, reaching the amount of the energy dissipation exceeding 2×10^5 W/m^2 at the field inclination around $50°-60°$. The heating contributions of high-frequency waves to the photosphere are almost constant, less dependent of the field inclination, and the amount is around $(2-6) \times 10^4$ W/m^2.

The dependency of the energy dissipation in the chromosphere is different from that observed in the photosphere. The energy dissipated in the chromosphere by the high-frequency waves decreases monotonically as a function of the field inclination; 8×10^3 W/m^2 in the inclination smaller than $30°$ and 3×10^3 W/m^2 in the inclination larger than $60°$. The energy by low-frequency waves increases with the field inclination in the range below $40°$, whereas the energy decreases in the range above $40°$. The maximum energy dissipation is 9×10^3 W/m^{-2} on average at the field inclination of $40°$, which may be slightly lower than the energy required for heating in the chromosphere. Jefferies et al. (2006) demonstrated that low-frequency waves propagate to the upper layers in the region where the magnetic field lines are inclined more than $30°$, but Figure 8(a) shows that the energy may not be carried efficiently to the chromospheric height when the magnetic field lines are more inclined beyond $40°$.

3.2.2. *Dependence on the inclination of magnetic field lines and field strength*

Figure 9 shows the energy dissipated in the chromosphere and photosphere with respect to the magnetic field strength (line of sight) and inclination. The field inclination is in $10°$ increments in the horizontal axis, and the field strength $|B|$ is in 100 G increments in the vertical axis. The energy dissipation values are the average of the data in four days.

For the amount of the dissipated energy estimated in the chromosphere, the low-frequency component shows an enhancement when the magnetic field lines with the magnitude higher than 600 G are inclined more than $40°$ (Figure 9(a)), while no apparent dependence on the inclination angle is observed for the high-frequency component (Figure 9(b)). The low-frequency and high-frequency components show less enhancements of the dissipated energy in the weak field pixels, which is different from behaviors in the photosphere as seen in Figure 8(c). The spectral profiles with single

(a) In the chromosphere (3 - 6 mHz)

(b) In the chromosphere (6 - 10 mHz)

(c) In the photosphere (3 - 6 mHz)

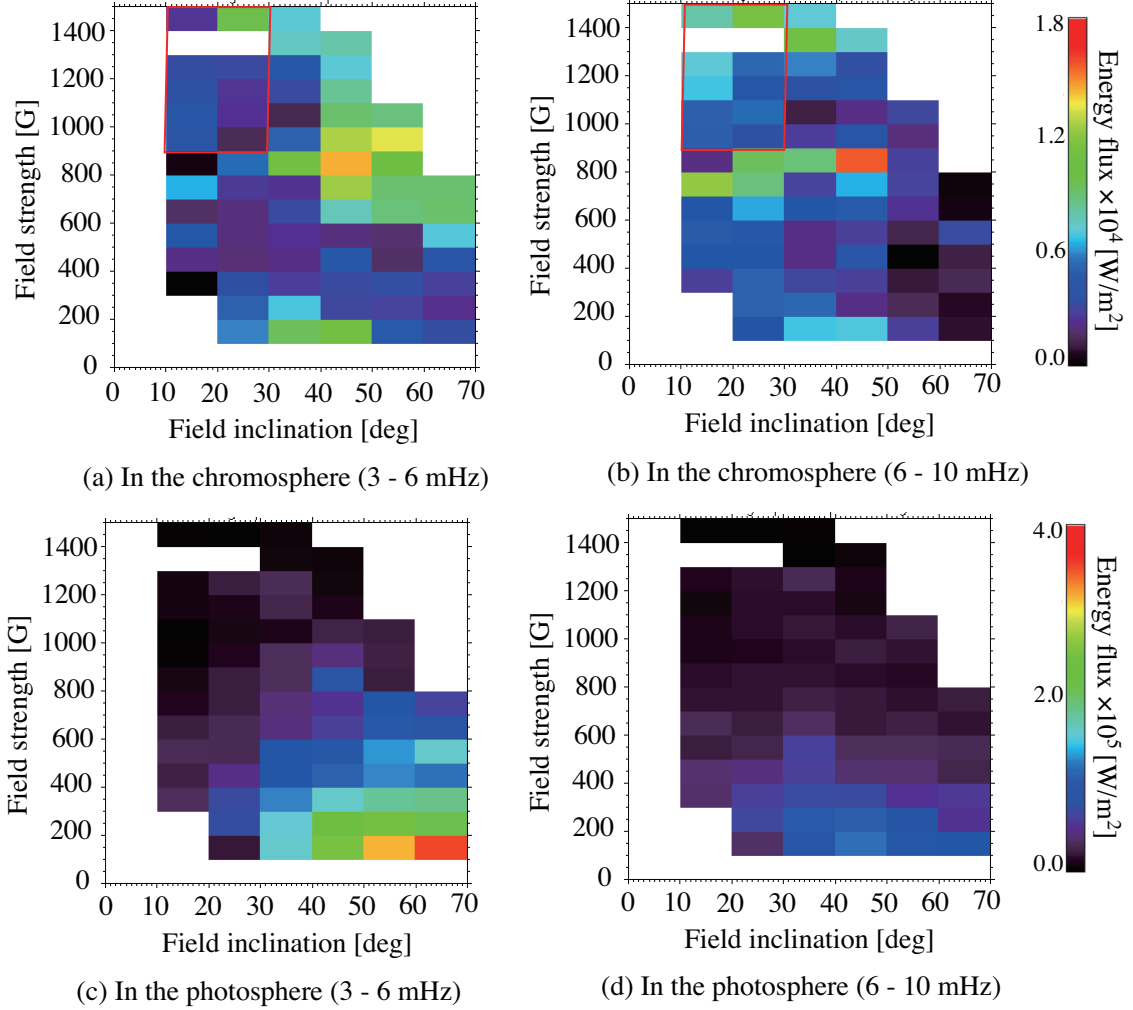(d) In the photosphere (6 - 10 mHz)

Figure 9. Amount of the dissipated energy as a function of the inclination of the magnetic field lines in the horizontal axis and the magnetic field strength in the vertical axis. (a) and (b) are the energy dissipated in the chromosphere by the low-frequency component (3-6 mHz) and the high-frequency component (6-10 mHz), respectively. (c) and (d) are the same but for the photosphere. The red box in (a) and (b) gives the condition where the line profile of Mg II k line is a single peak with only a tiny core inverted profile. The velocity for the upper chromosphere was derived by a whole profile fitting instead of the fitting to the core inverted profile as described in section 2.2. The values are acquired by averaging the data for four days.

or small amplitude peaks (Figure 2(c)) are observed mainly in the region marked by red box in Figures 9(a) and (b), indicating that they do not considerably affect the overall trend. If we focus on the energy dissipation in the photosphere, the energy dissipation of the low-frequency component is enhanced in the magnetic field below 600 G (Figure 9(c)). The enhanced energy dissipation is also

more significant as the field inclination increases. For the high-frequency component (Figure 9(d)), no significant enhancements are observed but the dissipated energy shows weak dependence on the field inclination, Also, the amount of energy dissipation is slightly enhanced in the magnetic field below 600 G. It is different from that observed in the low-frequency component.

The maximum magnitude of the energy dissipation by the low frequency component in the chromosphere is 1.4×10^4 W/m^2 (The value averaged over four days) at $40° < \theta < 60°$ and 800 G $< |B| < 1,000$ G. The dissipated energy may exceed 1×10^4 W/m^2 when the magnetic field with the strength higher than 600 G is inclined by 40 degree or more from the solar surface. This may satisfy the heating required for the chromosphere. The maximum energy dissipation in the photosphere is 3×10^5 W/m^2 (averaged over four days), which are distributed in weak (< 400 G) and inclined ($> 50°$) field pixels.

4. DISCUSSIONS

4.1. *Interpretations of the results*

As shown in Figure 9, the energy dissipation of the low-frequency component is more significant in the photosphere when the magnetic field is weaker than 400 G, while the chromosphere shows more energy dissipation by the low-frequency component when the magnetic field lines with the strength higher than 600 G are inclined more than $40°$ from the solar surface. On the photosphere, a large number of acoustic oscillation modes (p-modes) are mainly excited with periods of about 3-15 min (frequencies of about 1-5 mHz) and they are observed as the low-frequency component in weak magnetic field regions. Gas convection, which is the generator of magnetoacoustic waves at the photosphere, becomes weaker in the strong magnetic fields, making it harder for waves to be generated. The weak magnetic field region may contain isotropically propagating waves (fast mode of magnetoacoustic waves), which would dissipate before propagating to the chromosphere. As the amount of energy dissipation depends on the inclination of the magnetic field lines in the low-frequency component, the reduced effective gravity on the inclined magnetic field lines makes the cutoff frequency lower, allowing for the low-frequency component of the waves to propagate along the

magnetic field lines and to dissipate in the chromosphere. This interpretation suggests that the slow mode waves propagating along the magnetic field lines contribute significantly to the chromospheric heating. The left side of Figure 10 shows that fast-mode waves propagate isotropically in the weak magnetic field, and the center shows that high-frequency component can propagate upward into the chromosphere while low-frequency component is reflected below the cutoff frequency. The right side shows that low-frequency component can propagate upward because of lower cutoff frequency caused by the inclination of the magnetic field lines.
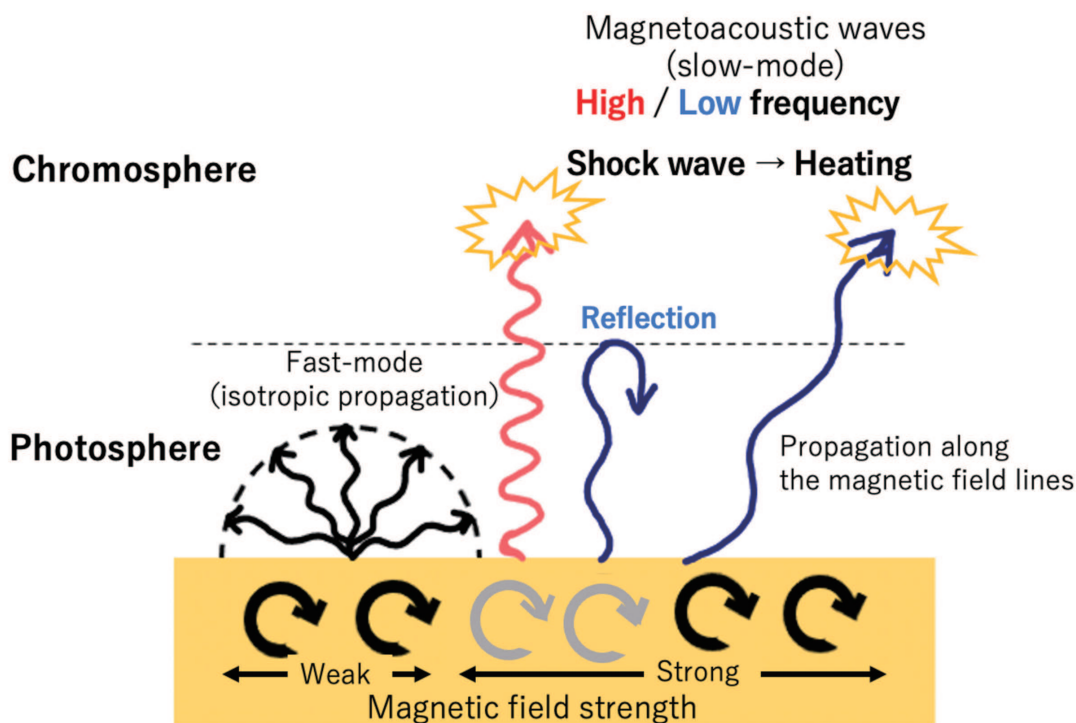

Figure 10. Waves inferred from results (schematic)

We have assumed here that the traveling waves generated by the photospheric convection heat the upper atmosphere; however, our analysis cannot provide the phase relations in the temporal profiles of velocities observed at each layer. Thus, we cannot give a definitive conclusion that the amount of energy obtained in this study is due to the dissipation of the traveling waves and their transformation into thermal energy. A part of velocity fluctuations may come from the waves reflected at the upper chromosphere and go downwards. There are two reasons why determining the phase relations in

velocity fluctuations measured at different heights is difficult; (1) when observing waves propagating along inclined magnetic field lines, the line-of-sight direction in the two measurements may not give the information on the same field line so that the same waves may not be captured at the two layers; (2) the chromosphere is full of plasma flows, making it difficult to distinguish the waves propagating from the photosphere. Figure 7(b) and (c) showed that the power in the magnetic field lines with $\theta > 50°$ is smaller than the others. This reduction may be partially explained by the Doppler velocity measurements as the line-of-sight component of waves propagating along the magnetic field lines.

For inclined magnetic field lines, the line-of-sight measurements at two layers may not derive the energy flux on the same magnetic field lines. As a trial, we shifted the observation position in the lower chromosphere (IRIS wing) by $1'' - 2''$ in the east-west direction from the original observation position and compared the power spectrum with that at the photosphere. The result demonstrated that the power spectrum in the lower chromosphere was larger than that in the photosphere for the low-frequency component depending on the observation position in the lower chromosphere. The data used herein have an extremely narrow field of view to increase the cadence, leading to difficulty in estimating the orientation of the inclined field lines. The 180-degree ambiguity resolution requires the spatial distribution of the field for a much wider field of view. To investigate the energy dissipation in more detail, tracing the magnetic field lines from the photosphere to the chromosphere is necessary. In the near future, the SUNRISE-3 experiment, that is, the third flight in series of the SUNRISE balloon-borne stratospheric observatory with a 1-m solar telescope (Barthol et al. 2011), is under planning for re-flight in 2024 and it will provide high-cadence series of spectro-polarimetric data for much wider field of view and with coverage from the photosphere to the chromosphere. Particularly, the Sunrise Chromospheric Infrared spectroPolarimeter (SCIP; Katsukawa et al. 2020) on the SUNRISE-3 experiment will be able to provide some spectral lines seamlessly covering from the photosphere through the middle chromosphere (Quintero Noda et al. 2017). Moreover, the focal plane instruments equipped to the ground-based 4-m Daniel K. Inouye Solar Telescope (DKIST), a facility of the National Solar Observatory (NSO), will provide similar series of spectro-polarimetric data.

The gas convection at the photosphere is a source of waves. The turbulent motions excite movement and deformation at the foot of the magnetic field lines. If the opposite polarity flux exists next to the field lines, they may approach each other and cause magnetic reconnection, i.e., nanoflares (Parker 1972), which may also generate another type of waves. Such a wave can contribute to velocity fluctuations. However, imagining that such a wave is included as the dominant source may be difficult because the energy dissipation of the low-frequency component increases with the inclination of the magnetic field lines, not only in the photosphere but also in the chromosphere at least with the inclined magnetic field up to 40 degree. Our results have been interpreted with slow mode waves as the most possible mechanism, but velocity fluctuations can also be created by Alfvén waves, which are a candidate for the heating of the corona. However, owing to the incompressible nature, Alfvén waves are unlikely to develop to shock waves in the chromosphere and may contribute little to the chromospheric heating.

4.2. *Formation height and density's assumption*

As described in Section 3.2, we used densities from the VAL-F atmospheric model to derive the energy flux in Figure 8. The VAL-F model is an atmospheric model for the bright inter-network that reproduces an atmosphere closer to the plage we have studied. Here we discuss at which height the three layers analyzed, i.e., the photosphere, the lower chromosphere, and the upper chromosphere, are located from the solar surface and evaluate how the estimated energy is sensitive to the assumption of density used in the calculation. The SP data is mostly sensitive to approximately 300 km from the solar surface, based on the formation height of the Fe I 6301.5 Å line, and thus, velocities from the SP were considered for the photospheric energy flux.

On the derivation of Doppler velocities at the lower and upper chromospheric layers, we used the wing and core profiles in the Mg II k line, respectively. To evaluate the height where the wing and core portions of the line are formed, we examined a publicly available simulation data cube from a realistic simulation of an enhanced network region (Carlsson et al. 2016). This simulation used the radiation magnetohydrodynamics code *Bifrost* (Gudiksen et al. 2011) to simulate the magnetic structure and dynamics of the outer atmosphere with a magnetic field topology characterized by two
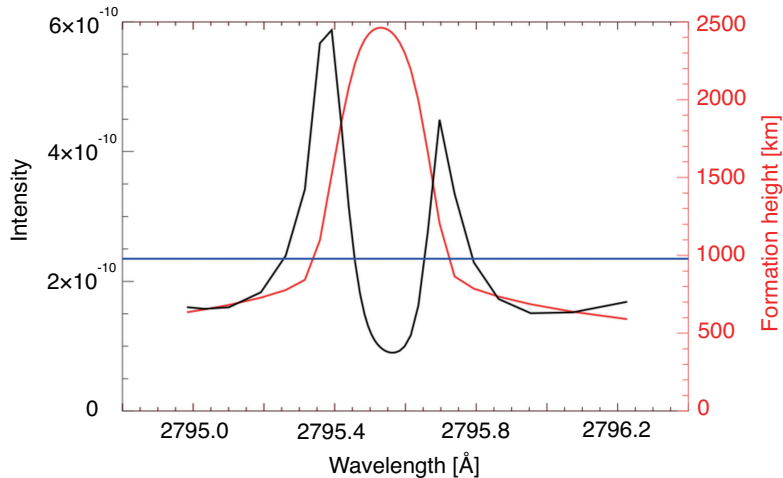
Figure 11. Spectral profile of the Mg II k line averaged over the field of view (black), and the height of the formation at each wavelength position of the line (red).

dominant opposite polarity islands separated by 8 Mm. The simulated magnetic field topology may be similar to what is observed in our plage regions located between two opposite polarity sunspots, although the spatial scale of the magnetic bipolar structure in the simulation is much smaller than that of our region. Nevertheless, we synthesized spectral profiles of the Mg II k line in a snapshot from this simulation for an enhanced network region by non-LTE radiative transfer computations with *RH* code (Uitenbroek 2001) and the method described in detail by Leenaarts et al. (2013b) and Hasegawa (2021). This computation enables us to study the heights where the wing and core of the Mg II k line are formed. Figure 11 shows the spectral profile averaged over the field of view in a snapshot and its height of the formation at each wavelength position in the central portion of the line. The wing portion for the lower chromosphere is formed at the height approximately 1,000 km, whereas 2,000–2,500 km for the line core that was fitted for the upper chromosphere. These values are only approximate because they are derived from the averaged spectral profile and are not identical to the actual atmosphere observed herein. As the chromosphere is thinner in the active region than in the quiet region, the density at 2,000 km (10,000 K) in VAL-F was assumed for the density in the upper chromosphere. When the formation height of the line core changes from 2,000 km (used in the results presented so far) to 1,800 km and 2,400 km in the VAL-F model, such difference in the

formation height of the line core provides a very minor change (less than 2 percent) in the evaluated energy dissipation in the chromosphere.

5. SUMMARY

In this study, we quantitatively estimated the magnetic field structure and derived how the energy dissipations at the photosphere and chromosphere depend on the properties of magnetic fields in the plage using the simultaneous observations by Hinode and IRIS. The results show that the energy dissipation by low-frequency waves at 3–6 mHz increases at the chromosphere in the range of the magnetic field inclination below 40 degree, and it begins to decrease when the field is more inclined beyond 40 degree. This is considered to be due to the propagation of low-frequency waves into the chromosphere. The effective gravity on the magnetic field lines decreases due to the tilt of the magnetic field lines, resulting in decreasing cutoff frequency. We interpreted that the waves observed in the chromosphere are mostly slow-mode waves propagating along the magnetic field lines. The low-frequency waves may be able to bring the energy in the vertical direction, although too highly inclined field may suppress the transport of energy in the vertical direction. The plage is observed to be bright in the chromosphere and is considered to be important for chromospheric heating. The previous studies, however, have not quantitatively described the energy dissipation above the plage as far as their authors know. Few studies have quantitatively utilized the magnetic field structure derived in the photosphere. The energy flux obtained by previous studies is less than the heating rate required for the chromosphere (Sobotka et al. 2016). In this study, we found that the low-frequency component in 3–6 mHz can dissipate more than 10^4 W/m² of energy in the chromosphere in only a specific configuration of the magnetic field lines. Furthermore, the amount of energy dissipated in the photosphere increases with decreasing magnetic field strength at the photosphere, whereas the

amount of energy dissipated in the chromosphere is more significant in the magnetic field strength higher than 600 G.

REFERENCES

Abbasvand, V., Sobotka, M., Heinzel, P., et al. 2020a, ApJ, 890, 22

Abbasvand, V., Sobotka, M., Švanda, M., et al. 2020b, A&A, 642, A52

Barthol, P., Gandorfer, A., Solanki, S. K., et al. 2011, Sol. Phys., 268, 1

Bel, N., & Leroy, B. 1977, A&A, 55, 239

Bloomfield, D., Lagg, A., & Solanki, S. 2007, ApJ, 671, 1005

Cally, P., & Moradi, H. 2013, MNRAS, 435, 2589

Carlsson, M., Hansteen, V. H., Gudiksen, B. V., Leenaarts, J., & De Pontieu, B. 2016, A&A, 585, A4

Carlsson, M., Leenaarts, J., & De Pontieu, B. 2015, ApJL, 809, L30

Cavallini, F. 2006, Sol. Phys., 236, 415

Centeno, R., Collados, M., & Trujillo Bueno, J. 2009, ApJ, 692, 1211

Chae, J., Park, H.-M., & Ahn, K. e. a. 2013, Solar Physics, 288, 1

De Pontieu, B., Rouppe van der Voort, L., Pereira, T. M. D., et al. 2014, in American Astronomical Society Meeting Abstracts, Vol. 224, American Astronomical Society Meeting Abstracts #224, 313.02

Felipe, T., Kuckein, C., & Thaler, I. 2018, A&A, 617, A39

Felipe, T., & Sangeetha, C. R. 2020, A&A, 640, A4

Graham, D. R., & Cauzzi, G. 2015, APJL, 807, L22

Gudiksen, B. V., Carlsson, M., Hansteen, V. H., et al. 2011, A&AP, 531, A154

Hasegawa, T. 2021, PhD thesis, The University of Tokyo

Heggland, L., Hansteen, V. H., De Pontieu, B., & Carlsson, M. 2011, ApJ, 743, 142

Ichimoto, K., Lites, B., Elmore, D., et al. 2008, Solar Physics, 249, 233

Jefferies, S. M., McIntosh, S. W., Armstrong, J. D., et al. 2006, ApJL, 648, L151

Jess, D. B. 2023, Living Reviews in Solar Physics, 20, 1

Jess, D. B., E., R. V., van Doorsselaere, T., Keys, P. H., & Mackay, D. H. 2013, ApJ, 779, 168

Kanoh, R., Shimizu, T., & Imada, S. 2016, ApJ, 831, 24

Katsukawa, Y., del Toro Iniesta, J. C., Solanki, S. K., et al. 2020, in Society of Photo-Optical Instrumentation Engineers (SPIE) Conference Series, Vol. 11447, Society of Photo-Optical Instrumentation Engineers (SPIE) Conference Series, 114470Y

Kosugi, T., Matsuzaki, K., Sakao, T., et al. 2007, Sol. Phys., 243, 3

Leenaarts, J., Pereira, T. M. D., Carlsson, M., Uitenbroek, H., & De Pontieu, B. 2013a, ApJ, 772, 89

—. 2013b, ApJ, 772, 90

Lites, B. W., & Ichimoto, K. 2013, Solar Physics, 283, 601

Lites, B. W., Akin, D. L., Card, G., et al. 2013, Sol. Phys., 283, 579

Löhner-Böttcher, J., & Bello González, N. 2015, A&A, 580, A53

McIntosh, S. W., & Jefferies, S. M. 2006, ApJL, 647, L77

Morrill, J. S., Dere, K. P., & Korendyke, C. M. 2001, ApJ, 557, 854

Oba, T., Iida, Y., & Shimizu, T. 2017, ApJ, 836, 40

Parker, E. N. 1972, ApJ, 174, 499

—. 1988, ApJ, 330, 474

Pereira, T. M. D., Leenaarts, J., De Pontieu, B., Carlsson, M., & Uitenbroek, H. 2013, ApJ, 778, 143

Pontin, D., & Hornig, G. 2020, Living Reviews in Solar Physics, 17, 5

Priest, E. 2014, Magnetohydrodynamics of the Sun (Cambridge University Press), doi:https://doi.org/10.1017/CBO9781139020732

Quintero Noda, C., Shimizu, T., & Katsukawa, Y. e. a. 2017, MNRAS, 464, 4534

Schmit, D., Bryans, P., De Pontieu, B., et al. 2015, ApJ, 811, 127

Schmitz, F., & Fleck, B. 1998, A&A, 337, 487

Schunker, H., & Cally, P. 2006, MNRAS, 372, 551

Shimizu, T., Nagata, S., Tsuneta, S., et al. 2008, Solar Physics, 249, 221

Sobotka, M., Heinzel, P., Švanda, M., et al. 2016, ApJ, 826, 49

Suematsu, Y., Tsuneta, S., Ichimoto, K., et al. 2008, Solar Physics, 249, 197

Title, A. M., Tarbell, T. D., Topka, K. P., et al. 1989, ApJ, 336, 475

Tsuneta, S., Ichimoto, K., Katsukawa, Y., et al. 2008, Sol. Phys., 249, 167

Uitenbroek, H. 2001, ApJ, 557, 389

Vernazza, J. E., Avrett, E. H., & Loeser, R. 1981, ApJS, 45, 635

von der Lühe, O. 1998, New Astron. Rev., 42, 493

Withbroe, G. L., & Noyes, R. W. 1977, ARA&A, 15, 363